



CHORUS

This is the accepted manuscript made available via CHORUS. The article has been published as:

Long-range dipole-dipole interaction and anomalous Förster energy transfer across a hyperbolic metamaterial

S.-A. Biehs, Vinod M. Menon, and G. S. Agarwal

Phys. Rev. B **93**, 245439 — Published 30 June 2016

DOI: [10.1103/PhysRevB.93.245439](https://doi.org/10.1103/PhysRevB.93.245439)

Long-Range Dipole-Dipole Interaction and Anomalous Förster Energy Transfer across Hyperbolic Meta Material

S.-A. Biehs*

Institut für Physik, Carl von Ossietzky Universität, D-26111 Oldenburg, Germany

**Corresponding author: s.age.biehs@uni-oldenburg.de*

Vinod M. Menon

Department of Physics, City College of New York, 160 Convent Ave New York, NY 10031, USA

G. S. Agarwal

Department of Physics, Oklahoma State University, Stillwater, Oklahoma 74078, USA

We study radiative energy transfer between a donor-acceptor pair across a hyperbolic metamaterial slab. We show that similar to a perfect lens a hyperbolic lens allows for giant energy transfer rates. For a realistic realization of a hyperbolic multilayer metamaterial we find an enhancement of up to three orders of magnitude with respect to the transfer rates across a plasmonic silver film of the same size especially for frequencies which coincide with the epsilon-near zero and the epsilon-near pole frequencies. Furthermore, we compare exact results based on the S-matrix method with results obtained from effective medium theory. Our finding of very large dipole-dipole interaction at distances of the order of a wavelength has important consequences for producing radiative heat transfer, quantum entanglement etc.

PACS numbers: 78.70.g,78.20Ci,42.50.p

I. INTRODUCTION

Dipole-dipole interactions are at the heart of many fundamental interactions such as van der Waals forces and vacuum friction [1, 2], Förster (radiative) energy transfer (FRET) [3, 4], radiative heat transfer [2, 5], quantum information protocols like the realization of CNOT gates [6–8], pairwise excitation of atoms [9–11], and Rydberg blockade [12, 13]. Clearly large number of problems in physics and chemistry require very significant dipole-dipole interaction at distances which are not much smaller than a wavelength. The development of plasmonic and metamaterial platforms can considerably enhance these fundamental dipole-dipole interactions. In an early work [14] it was shown that the dipole-dipole interaction [14, 15] can be quite significant even at distances bigger than microns if one utilizes whispering gallery modes of a sphere. More recently such systems have been revisited for their remarkable quantum features like squeezing [10]. Further it was shown that the energy transfer across plasmonic metal films can be enhanced [16] and that the long range plasmons allow for long-range plasmon assisted energy transfer between atoms placed on plasmonic structures such as graphene [17–19] and metals [20–24].

More elaborate structures possessing more features than simple single-layer plasmonic structures are for example hyperbolic metamaterials (HMM) [28, 29], which exhibit a broadband enhanced LDOS [30] allowing for broadband enhanced spontaneous emission [31–42], hyperbolic lensing [43–47], negative refraction [48, 49], super absorbers [50] and broadband enhanced thermal emission [51–56], for instance. These HMM can

be artificially fabricated by a periodic layout of sub-wavelength metal and dielectric components for applications in the visible. For applications in the infra-red phonon-polaritonic/semi-conductor and dielectric components can be combined [49, 52–55] but hyperbolic materials in the visible and infra-red also exist in nature [59–63]. Here we concentrate on artificially fabricated HMM since the choice of fabrication parameters makes it possible to control the epsilon-near zero (ENZ) and the epsilon-near pole (ENP) frequencies. At these frequencies the HMM can show extra-ordinary features as enhanced superradiance [64] and supercoupling [65, 66].

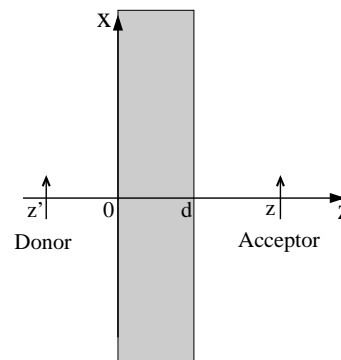


Figure 1: Sketch of the considered geometry. The metamaterial slab at the moment is an isotropic one with ϵ and μ as the dielectric and magnetic permeabilities.

The aim of our work is to study FRET across a hyperbolic multilayer metamaterial (see Fig. 1). We will demonstrate that similar to the perfect lens effect [67], the dipole-dipole interaction across a HMM can be en-

hanced by orders of magnitude compared to the pure plasmonic enhancement by a thin plasmonic metal layer. We will see that the enhancements are observed most strongly in the ENZ and ENP regime or in the type I HMM regime. This is the regime which is more easily accessible for experiments.

The organization of our paper is as follows: In Sec. II we introduce the elementary relations for FRET between a donor and an acceptor which are separated by an intermediate slab. We discuss the possibility of a perfect dipole-dipole interaction which is studied in Sec. III analytically and numerically for a thin silver film. Then, in Sec. IV, we discuss the anomalous transmission across a hyperbolic metamaterial as an alternative for realizing perfect dipole-dipole interaction. Finally, in Sec. V we study FRET across a concrete hyperbolic structure using exact S-matrix calculations. The exact numerical results are compared with the approximative results of effective medium theory.

II. POSSIBILITY OF PERFECT DIPOLE-DIPOLE INTERACTION

The Förster energy transfer rate between an donor-acceptor pair as sketched in Fig. 1 is well-known and can be written in terms of the dyadic Green's function \mathbf{G} as [4]

$$\Gamma = \int d\omega \sigma^{\text{abs}}(\omega) T(\omega) \sigma^{\text{em}}(\omega) \quad (1)$$

where σ^{abs} and σ^{em} are the absorption and emission spectra of the acceptor and donor and

$$T(\omega) = \frac{2\pi}{\hbar^2} \left(\frac{\omega^2}{\epsilon_0 c} \right)^2 |\mathbf{d}_D|^2 |\mathbf{d}_A|^2 |\mathbf{e}_A \cdot \mathbf{G} \cdot \mathbf{e}_D|^2 \quad (2)$$

introducing the dipole-transition matrix elements $\mathbf{d}_D = |\mathbf{d}_D| \mathbf{e}_D$ and $\mathbf{d}_A = |\mathbf{d}_A| \mathbf{e}_A$ of the donor and acceptor.

Making a plane wave expansion of the dyadic Green's function, we obtain

$$\mathbf{G}(\mathbf{r}, \mathbf{r}') = \int \frac{d^2\kappa}{(2\pi)^2} e^{i\kappa \cdot \mathbf{X}} \mathbf{G}(\boldsymbol{\kappa}, z) \quad (3)$$

where $\boldsymbol{\kappa} = (k_x, k_y)^t$, $\mathbf{X} = (x - x', y - y')^t$, and

$$\mathbf{G}(\boldsymbol{\kappa}, z) = \frac{ie^{i\gamma_v(z-z')}}{2\gamma_v} \left[t_s \mathbf{a}_s^+ \otimes \mathbf{a}_s^+ + t_p \mathbf{a}_p^+ \otimes \mathbf{a}_p^+ \right] \quad (4)$$

introducing the vacuum wavevector in z-direction $\gamma_v = \sqrt{k_v^2 - \kappa^2}$ and the vacuum wavenumber $k_v = \omega/c$. Note that the expression for the Green's function contains the contribution of the propagating ($\kappa < k_v$) and evanescent ($\kappa > k_v$) waves. The evanescent waves are exponentially decaying in z-direction so that during propagation these contributions are lost unless the medium somehow can reverse the decay of such waves. Here t_s and t_p are the

transmission coefficients of the s- and p polarization and $\mathbf{a}_{s,p}^+$ are the polarization vectors defined by

$$\mathbf{a}_s^+ = \frac{1}{\kappa} \begin{pmatrix} k_y \\ -k_x \\ 0 \end{pmatrix} \quad \text{and} \quad \mathbf{a}_p^+ = \frac{1}{\kappa k_v} \begin{pmatrix} -k_x \gamma_v \\ -k_y \gamma_v \\ \kappa^2 \end{pmatrix}. \quad (5)$$

The transmission coefficients for a metamaterial film can be expressed as [28, 67]

$$t_s = \frac{4\mu\gamma\gamma_v e^{i(\gamma-\gamma_v)d}}{(\gamma + \mu\gamma_v)^2 - (\gamma - \mu\gamma_v)^2 e^{2i\gamma d}}, \quad (6)$$

$$t_p = \frac{4\epsilon\gamma\gamma_v e^{i(\gamma-\gamma_v)d}}{(\gamma + \epsilon\gamma_v)^2 - (\gamma - \epsilon\gamma_v)^2 e^{2i\gamma d}}, \quad (7)$$

where the wavevector component inside the medium in z-direction is given by $\gamma = \sqrt{\epsilon\mu\omega^2/c^2 - \kappa^2}$. Note that the dipole-dipole interaction in free space (i.e. if we replace the film by vacuum) can be obtained from the Green's tensor in Eq. (4) by setting the transmission coefficients to one $t_s = t_p = 1$ (which is the result for $\epsilon = \mu = 1$), i.e.

$$\mathbf{G}^{(\text{vac})}(\boldsymbol{\kappa}, z) = \frac{ie^{i\gamma_v(z-z')}}{2\gamma_v} \left[\mathbf{a}_s^+ \otimes \mathbf{a}_s^+ + \mathbf{a}_p^+ \otimes \mathbf{a}_p^+ \right] \quad (8)$$

In this case the dipole-dipole interaction would become infinitely large if the donor and the acceptor would be placed at the same position, that means if $z = z'$. From a mathematical point of view this is so because the exponential prefactor equals one for $z = z'$ so that the κ -integral in Eq. (3) would diverge due to the fact that an infinite number of evanescent waves with $\kappa > k_v$ would contribute to the energy transfer. On the other hand, it is well known that the dipole-dipole interaction between the donor and acceptor is proportional to $1/|\mathbf{r}-\mathbf{r}'|^3$ which diverges for $z \rightarrow z'$, since we here have $x = x' = 0$ and $y = y' = 0$ as shown in the Fig. 1.

For an ideal left-handed material exhibiting negative refraction the permittivity and permeability are given by $\epsilon = \mu = -1$. In such a material evanescent plane waves are amplified as shown by Pendry when he introduced the concept of a perfect lens [67]. For the here defined transmission coefficients we obtain for $\epsilon = \mu = -1$

$$t_s = t_p = \exp(-2i\gamma_v d) \quad (9)$$

showing clearly the feature of amplification of evanescent waves inside the ideal left-handed material. Note, that this exponential amplification stems from the exponential in the denominator of the transmission coefficients. This is just the same expression derived by Pendry showing that for the perfect lens *both propagating and evanescent waves contribute to the resolution of the image* [67] which leads to the perfect lensing effect depicted in Fig. 2.

Inserting the expression of the transmission coefficients in the Green's tensor describing the dipole-dipole interaction gives

$$\mathbf{G}(\boldsymbol{\kappa}, z) = \frac{ie^{i\gamma_v(z-z'-2d)}}{2\gamma_v} \left[\mathbf{a}_s^+ \otimes \mathbf{a}_s^+ + \mathbf{a}_p^+ \otimes \mathbf{a}_p^+ \right]. \quad (10)$$

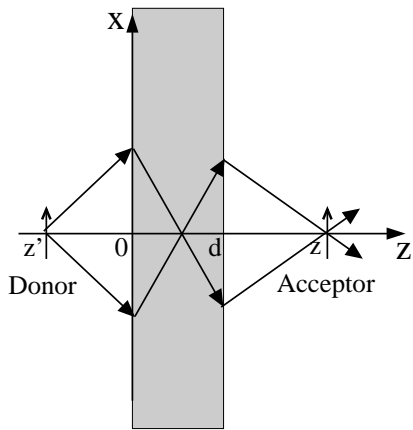


Figure 2: Sketch of the perfect lensing effect [67].

This Green's tensor is the same as expression (8) of the vacuum Green's tensor with the important difference that now the argument of the exponential prefactor is different. As in the case of interaction in free space we have an infinite large energy transfer if the exponential equals one leading to the condition that $z - z' = 2d$. Hence by placing the donor-acceptor pair such that this condition is fulfilled corresponds to a dipole-dipole interaction for two dipoles at the same position leading to an infinitely large energy transfer rate. This is so, because for $z - z' = 2d$ all evanescent waves ($\kappa > k_v$) get focused. We have thus shown that a perfect negative material with zero losses can yield perfect dipole-dipole interaction and perfect energy transfer which is limited only by the donor and acceptor line shapes.

III. SILVER FILM AS METAMATERIAL

As pointed out by Pendry [67] for observing the perfect lensing effect it suffices to consider a thin silver film. In the quasistatic-limit such a thin silver film mimicks a perfect lens for the p-polarized waves at a frequency ω_{pl} where $\epsilon'(\omega_{pl}) = -1$, which coincides with the surface plasmon resonance frequency of a single metal interface. To see this we take the quasi-static limit ($\kappa \rightarrow \infty$) of the transmission coefficient t_p in Eq. (7) with $\mu = 1$. We obtain

$$t_p \rightarrow \frac{4\epsilon}{(\epsilon + 1)^2 - (\epsilon - 1)^2 e^{2i\gamma d}}. \quad (11)$$

The exponential in the numerator vanishes because in the quasi-static limit $\gamma_v \approx \gamma \approx i\kappa$. If we now insert

$$\epsilon = -1 + i\epsilon'', \quad (12)$$

then we arrive at

$$t_p \rightarrow \frac{4(i\epsilon'' - 1)}{\epsilon''^2 (e^{2i\gamma d} - 1) + 4(i\epsilon'' - 1)e^{2i\gamma d}}. \quad (13)$$

It is now easy to see that for vanishing losses $\epsilon'' \rightarrow 0$ we again have ($\gamma_v \approx \gamma \approx i\kappa$)

$$t_p = \exp(-2i\gamma_v d). \quad (14)$$

Proving that a silver film can mimick a perfect lens. The only drawback is that in metals the losses are not negligible so that the perfect lens effect does not persist in this case. Nonetheless even with losses one can expect to find large Förster energy transfer due to the fact that the donor and acceptor can couple to the surface waves inside the silver film.

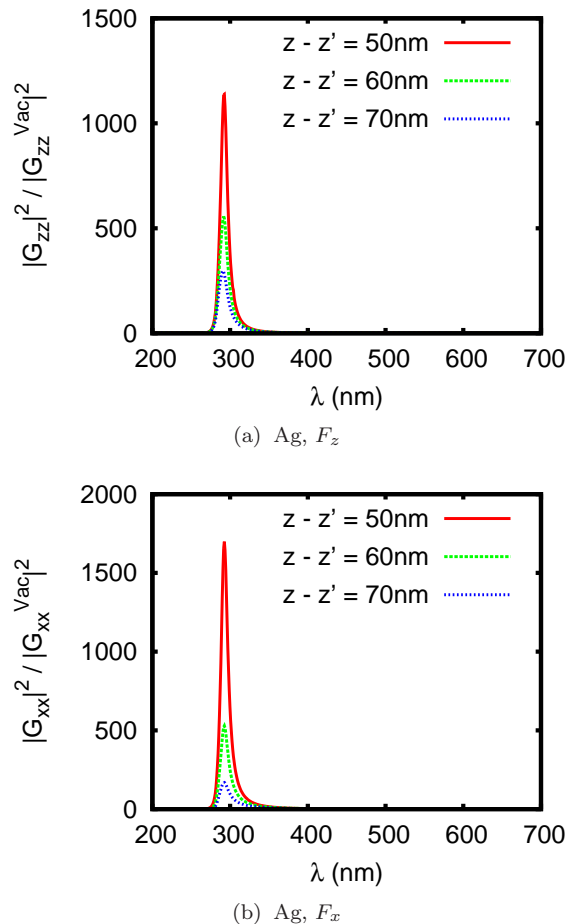


Figure 3: Plot of F_z and F_x as function of wavelength for a silver film with thickness $d = 30$ nm. The donor is placed at $z' = -10$ nm and the position of the acceptor is varied such that $z - z' = 50$ nm, 60 nm, 70 nm.

That the coupling to the surface plasmons can enhance the energy transfer has been demonstrated theoretically for different systems like nanoparticles [68], plasmonic waveguides [23] and films [20, 21] as well as graphene [17–19]. This enhanced energy transfer might be exploited for solar energy conversion [22]. Experimentally it has been shown by Viger et al. [69] and Zhang et al. [70] that plasmonic nanoparticles can enhance the energy transfer rate; Andrew and Barnes [16] have proven experimentally

that the Förster energy transfer across thin silver films can be enhanced by the coupling to the surface plasmon polaritons demonstrating a long-range coupling between the donor-acceptor pair across films with thicknesses up to 120nm. Although we are here particularly interested in the long-range energy transfer across a film, surface plasmons can also be used to mediate the energy transfer along plasmonic structures as shown theoretically [17–21, 23]. Recently, Bouchet *et al.* [24] have detected this long-range energy transfer when both donor and acceptor are placed on a plasmonic platform like a thin metal film.

To see how the Förster energy transfer is affected by the presence of a metal film, we consider therefore first a thin silver layer with permittivity described by the Drude model

$$\epsilon_{\text{Ag}} = \epsilon_{\infty} - \frac{\omega_p^2}{\omega(\omega + i\tau^{-1})}. \quad (15)$$

For silver the parameters from [25, 26] are $\epsilon_{\infty} = 3.7$, $\omega_p = 1.4 \cdot 10^{16}$ rad/s, $\tau = 4 \cdot 10^{-14}$ s. However, we use a much smaller relaxation time of $\tau = 0.45 \cdot 10^{-14}$ s which accounts for the increased collision frequency found in thin metal films [27]. Note that a reduced relaxation time results in reduced energy transfer rates. In order to quantify the enhancement of the energy transfer we introduce the enhancement factor

$$F_i \equiv \frac{|G_{ii}|^2}{|G_{ii}^{(\text{vac})}|^2}, \quad (16)$$

where $i = x, z$ is the orientation of the dipole-transition matrix element of the donor/acceptor and $G_{ii}^{(\text{vac})}$ is the vacuum Green's function. In Fig. 3 we show our results for the enhancement of the dipole-dipole interaction due to the presence of a silver film of thickness $d = 30$ nm with respect to the case where this film is replaced by vacuum. It can be seen that the dipole-dipole interaction and therefore the Förster energy transfer is especially large for $\lambda \approx 300$ nm where $\epsilon'_{\text{Ag}} \approx -1$ as expected. Furthermore it can be seen that at $z - z' = 2d = 60$ nm no particular effect happens proving that losses mask the perfect lens effect. The Förster energy transfer becomes just less important when the distance $z - z'$ between the donor-acceptor pair is increased. In Fig. 4 we show similar results for a much thicker film with $d = 120$ nm. In this case there can be still seen an enhancement effect for z orientation but of course the enhancement effect becomes less important when the thickness of the silver film is increased due the losses inside the metal film. Therefore another kind of material is needed in order to overcome the harmful effect of the losses. Nonetheless such an enhancement due to the surface plasmons of the silver film have already been measured in the experiment by Andrew and Barnes [16] for film thicknesses of $d = 30$ nm, 60 nm, 90 nm and even $d = 120$ nm.

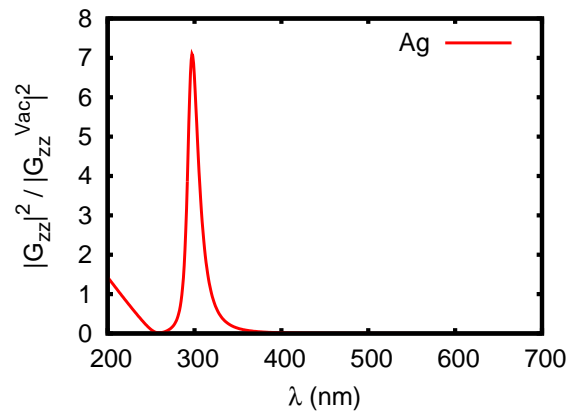
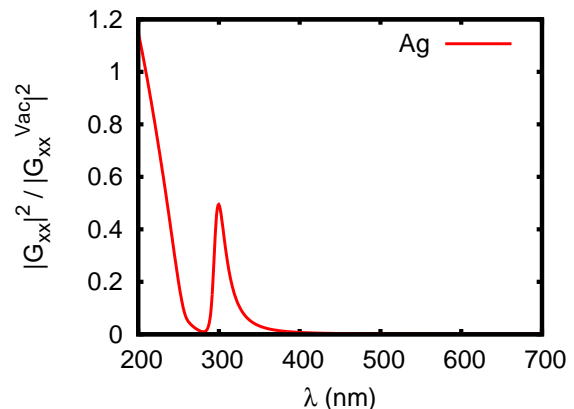
(a) Ag, F_z (b) Ag, F_x

Figure 4: Plot of F_z and F_x as function of wavelength. The donor and acceptor are placed in a distance of 10 nm of each interface (i.e. $z' = -10$ nm and $z - d = 10$ nm) of a silver film with thickness $d = 120$ nm.

IV. ANOMALOUS TRANSMISSION FOR HYPERBOLIC MATERIALS

Now, let us replace the ideal left-handed material slab by a hyperbolic or indefinite material [29]. The beauty of such hyperbolic materials is that waves with large kappa ($\kappa \gg k_v$) emitted by a donor which would be evanescent in free space are homogenous within these materials. This leads to significant fields on the other side of the slab which makes hyperbolic materials very advantageous for energy transfer even for slabs with an appreciable thickness as was shown in some preliminary works [57, 58] carried out solely in the hyperbolic dispersion region. This is to contrast with our work which addresses ENZ and ENP regions where we see the maximum enhancements. Hyperbolic materials are uni-axial materials which do exist in nature [59–63]. But they can also be easily fabricated by combining alternating layers of dielectric and plasmonic materials in a periodic structure, for instance. Here, we consider only the non-magnetic case so that the permeability tensor is given by the unit tensor and the

permittivity tensor is given by $\text{diag}(\epsilon_{\perp}, \epsilon_{\perp}, \epsilon_{\parallel})$ with respect to the principal axis. In our case the z -axis is the optical axis of the uni-axial material. The dispersion relations of the ordinary and extra-ordinary modes inside the uni-axial medium are [71]

$$\frac{\gamma_o^2}{\epsilon_{\perp}} + \frac{\kappa^2}{\epsilon_{\perp}} = k_v^2 \quad \text{and} \quad \frac{\gamma_e^2}{\epsilon_{\perp}} + \frac{\kappa^2}{\epsilon_{\parallel}} = k_v^2 \quad (17)$$

where γ_o (γ_e) is the z -component of the wavevector of the ordinary (extraordinary) mode. Neglecting dissipation for a moment we can easily define normal dielectric uni-axial materials as materials with $\epsilon_{\parallel} > 0$ and $\epsilon_{\perp} > 0$ and hyperbolic materials as materials with $\epsilon_{\parallel}\epsilon_{\perp} < 0$, i.e. one of both permittivities is positive and the other one negative. Due to the property $\epsilon_{\parallel} > 0$ and $\epsilon_{\perp} > 0$ the iso-frequency curves for dielectric uni-axial materials in k -space are ellipsoids whereas for hyperbolic materials these iso-frequency curves are hyperboloids. For $\epsilon_{\parallel} < 0$ and $\epsilon_{\perp} > 0$ — a type I hyperbolic material — the iso-frequency curve is a two-sheeted hyperboloid and for $\epsilon_{\parallel} > 0$ and $\epsilon_{\perp} < 0$ — a type II hyperbolic material — the iso-frequency curve is a one-sheeted hyperboloid. In Fig. 5 the iso-frequency lines of a type I hyperbolic material are sketched in the k_z - k_x plane.

Now we will show that similar to the perfect lensing effect the evanescent waves can be amplified inside a hyperbolic slab even in the absence of a magnetic response. To this end, we consider the transmission coefficients of a uniaxial slab where the optical axis is normal to the interface, i.e. it is along the z -axis. In this case the transmission coefficients for the ordinary and extraordinary modes (which coincide with the s - and p -polarized modes) are given by

$$t_s = \frac{4\gamma_o\gamma_v e^{i(\gamma_o - \gamma_v)d}}{(\gamma_o + \gamma_v)^2 - (\gamma_o - \gamma_v)^2 e^{2i\gamma_o d}} \quad (18)$$

$$t_p = \frac{4\epsilon_{\perp}\gamma_e\gamma_v e^{i(\gamma_e - \gamma_v)d}}{(\gamma_e + \epsilon_{\perp}\gamma_v)^2 - (\gamma_e - \epsilon_{\perp}\gamma_v)^2 e^{2i\gamma_e d}}. \quad (19)$$

The effect of anisotropy is mainly seen in the transmission coefficient t_p because only here both permittivities ϵ_{\perp} and ϵ_{\parallel} enter. When considering an epsilon-near-zero (ENZ) material with $\epsilon_{\perp} \rightarrow 0$, then $\gamma_o, \gamma_e \rightarrow 0$ so that the exponential in the denominator of t_s and t_p is one and we find

$$t_s \rightarrow e^{-i\gamma_v d} \quad \text{and} \quad t_p \rightarrow e^{-i\gamma_v d}. \quad (20)$$

That means that similar to the perfect lensing effect, the evanescent waves are amplified by uni-axial material and in particular by a hyperbolic structure. Note, that this time the exponential which enhances the evanescent modes stems from the numerator of the transmission coefficient which makes this effect more robust against losses. Similarly, when considering an epsilon-near-pole (ENP) material with $\epsilon_{\parallel} \rightarrow \infty$, then t_s remains unaffected because γ_o remains unaltered. But for the extra-ordinary

wave we have $\gamma_e \approx \sqrt{\epsilon_{\perp}}\omega/c$. It follows that

$$t_p \rightarrow A e^{-i\gamma_v d} \quad (21)$$

with

$$A \equiv \frac{4\epsilon_{\perp}\sqrt{\epsilon_{\perp}}k_v\gamma_v e^{ik_v\sqrt{\epsilon_{\perp}}d}}{(k_v\sqrt{\epsilon_{\perp}} + \epsilon_{\perp}\gamma_v)^2 - (k_v\sqrt{\epsilon_{\perp}} - \epsilon_{\perp}\gamma_v)^2 e^{2ik_v\sqrt{\epsilon_{\perp}}d}}. \quad (22)$$

Therefore $t_p \propto \exp(-i\gamma_v d)$ and the evanescent modes are again amplified, if the κ -dependent prefactor A is not too small.

To summarize, we find that for ENZ and ENP frequencies evanescent waves in vacuum are amplified and the dipole-dipole interaction can at least in principle become infinitely large if $z = z' + d$, i.e. if the donor and the acceptor are both exactly deposited on the surface of the hyperbolic film which cannot be achieved in a real setup. But even if this condition is not perfectly met, we can expect to find an amplified energy transfer across a hyperbolic slab at the ENZ and ENP frequencies. Furthermore, from the above derivation suggests that the ENZ resonance is more advantageous for transmission than the ENP resonance, because the prefactor fullfills for $\epsilon > 0$ typically $|A| < 1$.

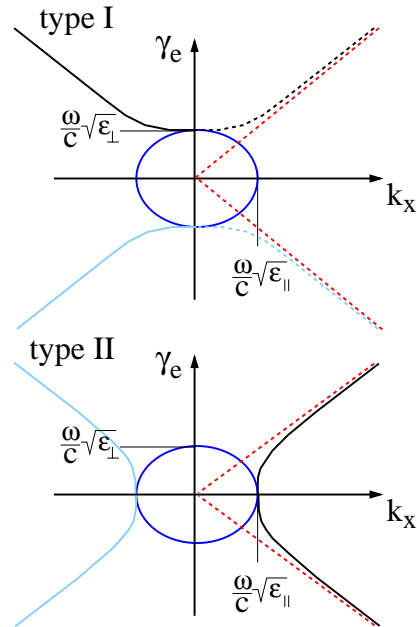


Figure 5: Sketch of the isofrequency lines of γ_e for a dielectric uniaxial medium (blue ellipse) and a type I/II hyperbolic material (solid black and light blue line). The asymptotes (dashed red lines) are given by $k_z = \pm k_x \sqrt{|\epsilon_{\perp}|/|\epsilon_{\parallel}|}$.

Note, that both regimes of ENZ and ENP were discussed in the context of diffraction suppressed hyperbolic lensing [44], using the canalization regime for hyperbolic lensing [72, 73] and directed dipole emission [45]. In these cases, the advantage of using ENZ and ENP resonances lies in the resulting very flat iso-frequency line of the extra-ordinary modes so that the group velocity is mainly

directed along the optical axis for a very broad band of lateral wavenumbers κ . This becomes clear when looking at the asymptotes of the isofrequency lines of γ_e as shown in Fig. 5. For large wavenumbers κ (evanescent regime) we have $\gamma_e \approx \kappa \sqrt{|\epsilon_{\perp}|/|\epsilon_{\parallel}|}$. With this result we can evaluate the ratio of the group velocity along the z-axis and the group velocity perpendicular to the z-axis and obtain

$$\left| \frac{\frac{d\omega}{d\gamma_e}}{\frac{d\omega}{d\kappa}} \right| = \left| \frac{\gamma_e \epsilon_{\parallel}}{\kappa \epsilon_{\perp}} \right| \approx \sqrt{\frac{|\epsilon_{\parallel}|}{|\epsilon_{\perp}|}}. \quad (23)$$

Hence, at the ENZ and ENP resonance the slope of the isofrequency lines become infinitely small and the group velocity becomes mainly directed parallel to the optical axis so that the energy transferred between the donor and acceptor flows preferentially along the line connecting both, if both are placed along the optical axis.

V. S-MATRIX CALCULATION OF THE DIPOLE-DIPOLE INTERACTION

Let us turn to a concrete numerical example. We consider a hyperbolic multilayer metamaterial made of alternating layers of silver and TiO_2 which has for example been used in the experiment in Ref. [40]. In most treatments of such multilayer materials, effective medium theory (EMT) is used which describes the multilayer structure as a homogenous but uni-axial material, with an optical axis perpendicular to the interfaces. Within EMT the effective permittivities of the multilayer structure can be easily calculated and are given by

$$\epsilon_{\perp} = f\epsilon_{\text{Ag}} + (1-f)\epsilon_{\text{TiO}_2}, \quad (24)$$

$$\epsilon_{\parallel} = \frac{\epsilon_{\text{Ag}}\epsilon_{\text{TiO}_2}}{f\epsilon_{\text{TiO}_2} + (1-f)\epsilon_{\text{Ag}}}, \quad (25)$$

where f is the filling fraction of silver and $\epsilon_{\text{Ag}}/\epsilon_{\text{TiO}_2}$ are the permittivities of the both constituents of the multilayer structure. For silver we use the Drude model in Eq. (15). TiO_2 is transparent in the visible regime. It's permittivity ϵ_{TiO_2} is nearly constant in that regime and can be well described by the formula [76]

$$\epsilon_{\text{TiO}_2} = 5.913 + \frac{0.2441}{\lambda^2 - 0.0803}. \quad (26)$$

where λ is the wavelength in micrometer. The effective permittivities ϵ_{\perp} and ϵ_{\parallel} are shown in Fig. 6 for a filling fraction of $f = 0.35$. It can be seen that at the edges of the hyperbolic bands we find the ENP and ENZ points at $\lambda = 394.8$ nm and $\lambda = 551.2$ nm. To make these points more obvious we show in Fig. 6 a plot of $|\epsilon_{\perp}|/|\epsilon_{\parallel}|$. By changing the filling fraction the position of the ENZ and ENP frequencies can be shifted. Note that the strong resonance in the type I regime around $\lambda = 350$ nm can essentially be considered as an ENZ resonance, since for large κ it converges to the ENZ point as can be seen in Fig. 6. When increasing the filling fraction the dielectric

band in between both hyperbolic bands in Fig. 6 will become smaller until $f = 0.5$, then the frequencies of ENP and ENZ coincide since in this case both hyperbolic bands (type I and type II) are in juxtaposition with each other.

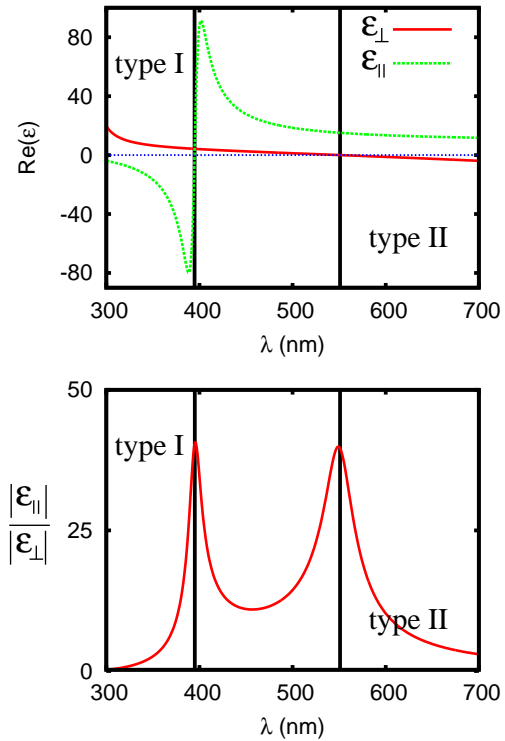


Figure 6: Top: plot of the real part of the effective permittivities ϵ_{\perp} and ϵ_{\parallel} for a Ag/ TiO_2 multilayer hyperbolic material with a silver filling fraction of $f = 0.35$. The vertical lines mark the edges of the hyperbolic bands of type I and type II. Bottom: plot of $|\epsilon_{\parallel}|/|\epsilon_{\perp}|$ manifesting the ENP and ENZ points at $\lambda = 394.8$ nm and $\lambda = 551.2$ nm.

However, the EMT is only applicable if the considered wavelengths and distances are much larger than the period of the multilayer structure [35, 36, 36, 38, 74]. Furthermore, EMT cannot account for the ordering of the layers so that it can be very important if we consider a finite Ag/ TiO_2 or TiO_2/Ag multilayer material [74]. Therefore we will use mainly full S-matrix calculations [75] to determine the transmission coefficients of the multilayer hyperbolic film. Here, we choose silver as first layer which is facing the donor. Hence, the last layer facing the acceptor is made of TiO_2 .

The transmission coefficient of the extra-ordinary waves t_p is plotted in Fig. 7 for a Ag/ TiO_2 multilayer structure of thickness $d = 120$ with a filling fraction of $f = 0.35$ of silver. The calculation was made for $N = 24$ layers, which means that the silver layers have a thickness of 3.5nm and the TiO_2 layers have a thickness of 6.5nm which is at the lower limit of a realizable structure. In Fig. 7 the different coupled surface modes of the hyperbolic multilayer structure can be seen. Obviously

in the type I hyperbolic band the coupled surface modes can exhibit negative group velocities which will result in negative refraction [49]. Furthermore it can be nicely seen that all the coupled modes converge for large κd towards the ENZ and ENP frequencies (vertical lines). Therefore at those ENZ and ENP frequencies we have quite a number of surface modes with zero group velocity in direction of the interfaces of the multilayer structure. These are the waves which will contribute dominantly to the Förster energy transfer having a group velocity rather along the optical axis (z -direction) than perpendicular to it as shown in Eq. (23). This is so, because for the evanescent waves with large $\kappa \gg k_v$ the exponentials in the Green's function in Eq. (4) introduce a cutoff [79] at $\kappa \approx 1/(z - z' - d)$ at the ENP and ENZ frequencies for the κ -integral, since $t_p \approx \exp(\kappa d)$ in this case. Therefore the major contributions stem from κ around $1/(z - z' - d)$. That means in the ideal case $z - z' = d$ all evanescent waves contribute, but in the non-ideal realistic case only evanescent waves up to a finite value of $\kappa \approx 1/(z - z' - d)$ will contribute to the energy transfer.

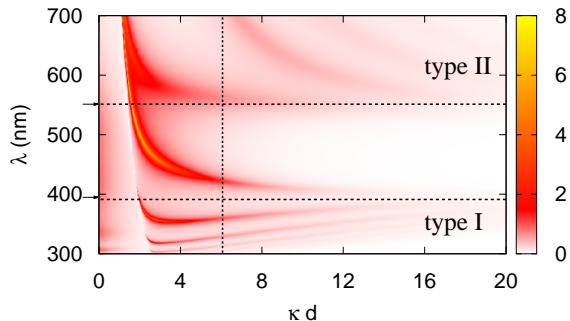


Figure 7: Plot of the transmission coefficient $|t_p \exp(-\kappa d)|^2$ for the hyperbolic Ag/TiO₂ multilayer structure $d = 120$ nm and $N = 24$ with filling fraction of $f = 0.35$. We have multiplied the transmission coefficient with $\exp(-\kappa d)$ to compensate the exponential enhancement of the evanescent waves with large $\kappa \gg \frac{\omega}{c}$. The horizontal lines and arrows mark the edges of the hyperbolic bands.

In Fig. 8 we show now the results for the enhancement factors F_x and F_z of the Förster energy transfer by a Ag/TiO₂ hyperbolic multilayer structure. It can be seen that the enhancement is especially large close to the ENZ and ENP frequencies. Furthermore, the enhancement is more than two orders of magnitude larger than for a single silver film in Fig. 4, so that this enhancement of energy transfer due to the ENP and ENZ resonances is much larger than the enhancement due to the thin film surface plasmons. Since the latter has already been measured by Andrew and Barnes [16] the ENP and ENZ enhancement should be easily measurable. The advantage of the hyperbolic structures to have large energy transfer over long distances becomes apparent when comparing

configuration	F_z	F_z
	$(z - z' = 50 \text{ nm})$	$(z - z' = 140 \text{ nm})$
Ag, $d = 30$ nm (SPP)	1138	25
Ag, $d = 120$ nm (SPP)	-	7.1
HMM, N6, (typeI)	-	241
HMM, N6, (ENP)	-	268
HMM, N8, (typeI)	-	518
HMM, N8, (ENP)	-	380
HMM, N10, (typeI)	-	725
HMM, N10, (ENP)	-	428
HMM, N10, (ENZ)	-	115
HMM, N12, (typeI)	-	873
HMM, N12, (ENP)	-	452
HMM, N12, (ENZ)	-	164
HMM, N24, (typeI)	-	1204
HMM, N24, (ENP)	-	477
HMM, N24, (ENZ)	-	493

Table I: Collection of the enhancement factors F_z for silver films (with $d = 30$ nm and $d = 120$ nm) and HMMs (with different number of layers N , but all have a thickness of $d = 120$ nm) close to the surface plasmon polariton resonance frequency (SPP), the resonances at the ENP and ENZ points as well as the ENZ resonance in the type I regime (near $\lambda = 350$ nm). In all cases the distance of the donor and acceptor to the surface is the same (i.e. we consider the symmetric situation where $|z'| = z - d$).

the different enhancement factors listed in Table I. Of course, this hyperbolic enhancement effect also exists for much thicker structures. Note, that by increasing the number of layer N in the multilayer film or by increasing the distance of the donor-acceptor pair with respect to the film the exact S-matrix result converges to the EMT result. Realization of ultrathin layers for realizing hyperbolic materials is not very practical. However even in that case if one was to compare the performance of a single silver film versus the hyperbolic material using EMT or numerical calculation, one will find that while thin silver performs much better close to the volume plasmon frequency of silver (300 nm), at longer and more practical wavelengths where donor molecules are found, the HMM does a better job. Additionally, the use of multilayered structures also allows one to tune the frequency range where hyperbolic dispersion occurs through control of fill fraction and thereby engineer the spectral range at which the energy transfer enhancement is desired.

The position of the peaks can be explained by the fact that the dominant contributions to the energy transfer stem from $\kappa d \approx d/(z - z' - d) = 6$ in this case. The vertical line in Fig. 7 is exactly at this value. It can be seen that the frequencies at which the coupled surface modes cross this vertical line coincide with the resonances of the energy transmission in Fig. 8. If we would increase the donor-acceptor distance $z - z'$ the vertical line would

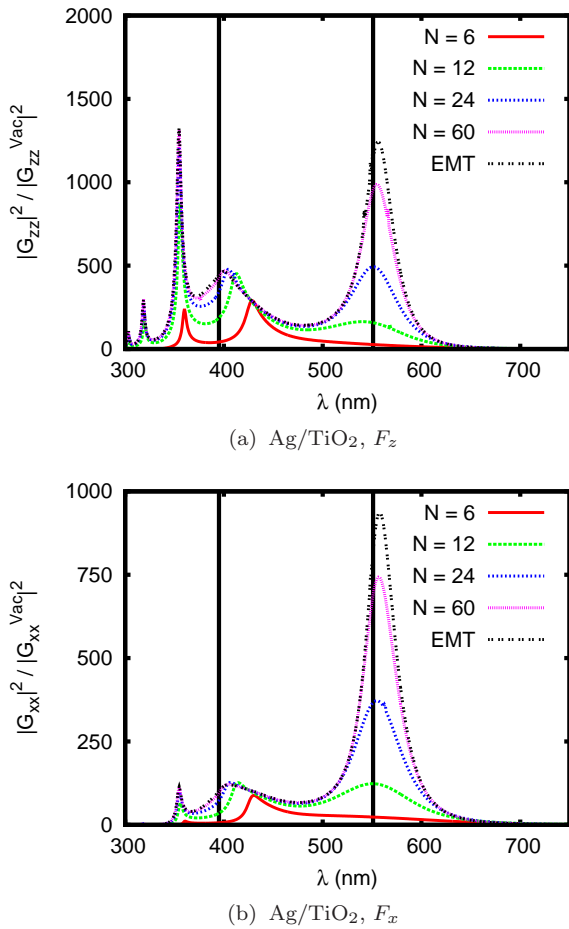


Figure 8: Plot of F_z and F_x as function of wavelength. Again donor and acceptor are placed in a distance of 10 nm of each interface (i.e. $z' = -10$ nm and $z - d = 10$ nm) of the film of thickness $d = 120$ nm. Here the film is given by a Ag/TiO₂ multilayer structure with $N = 6, 12, 24, 60$ layers. The filling fraction of silver is $f = 0.35$. For comparison the exact and the EMT results are shown. The vertical lines correspond again to the edges of the hyperbolic bands as in Fig. 6.

move to smaller κ values in Fig. 7 so that the resonances will shift accordingly. This shifting of the resonances is shown in Fig. 9(a). Obviously, the enhancement around the ENZ and ENP frequencies gets smaller and smaller, when the distance of the donor and acceptor with respect to the surface is increased. However as can be seen in Fig. 10, there can still be an enhancement of 30 for the energy transfer inside the type I hyperbolic band if the distance of the donor and acceptor with respect to the surface of the hyperbolic medium has relative large values as for example 100 nm so that $z - z' = 320$ nm.

Finally, we also consider the influence of a 10 nm silica cladding which is deposited on the metal layer on the donor-side of the structure. Obviously the cladding improves the performance of the hyperbolic multilayer structure, because waves which are evenescient in air/vacuum when there is no cladding can be homo-

geneous inside the cladding. Therefore, the light from the donor couples better into the structure when there is a cladding due to the increased density of states in the dielectric compared to air - hence the emission pattern gets modified leading to an increased energy transfer. So far we have not included the absorption and emission line shapes of the acceptor and donor. We next show that such an inclusion does not change the enhancement factors much. We include explicitly the case when the donor emission peak is near 550 nm. The emission and absorption shapes are modeled as Lorentzians:

$$\sigma^{\text{em}}(\omega) = \frac{1}{\pi} \frac{\Gamma_0}{(\omega - \omega_0)^2 + \Gamma_0^2}, \quad (27)$$

$$\sigma^{\text{abs}}(\omega) = \frac{1}{\pi} \frac{\Gamma_0}{(\omega - \bar{\omega})^2 + \Gamma_0^2} \quad (28)$$

with $\bar{\lambda} = \lambda_0 + \Delta$ ($\omega_0 = 2\pi c/\lambda_0$ and $\bar{\omega} = 2\pi c/\bar{\lambda}$) using the realistic parameters $\Delta = 30$ nm and $\Gamma_0 = 2.28 \times 10^{14} \text{ s}^{-1}$. Then the enhancement factor can be expressed as [confer with Eq. (1)]

$$\bar{F}_i := \frac{\int d\omega \sigma^{\text{em}}(\omega) \sigma^{\text{abs}}(\omega) |G_{ii}|^2 \omega^4}{\int d\omega \sigma^{\text{em}}(\omega) \sigma^{\text{abs}}(\omega) |G_{ii}^{(\text{vac})}|^2 \omega^4}. \quad (29)$$

A plot of the numerical result in Fig. 9(c) for donor-acceptor pairs with λ_0 and $\bar{\lambda}$ around one of the resonant transmission peaks at 550 nm shows that due to the broad-band enhancement of the transmission through the hyperbolic material the enhancement factor is at its maximum about 900 which is quite close to the predicted maximal enhancement factor of 1330 in Fig. 9(b).

VI. CONCLUSION

In conclusion, we have discussed the perfect lens effect and its pendant for hyperbolic metamaterials in the context of Förster energy transfer between a donor-acceptor pair placed on each side of the perfect or hyperbolic lens. We have demonstrated that in principle in both cases one can have an infinitely large dipole-dipole interaction for precisely defined positions of the donor-acceptor pair and well-defined frequencies which coincide with the surface plasmon frequency in the case of a perfect lens and the epsilon-near zero or epsilon-near infinity frequency for the hyperbolic lens. Due to losses this interactions becomes finite but it remains large compared to the dipole-dipole interaction in vacuum. The main reason for such large enhancements is that the enhancement effect in HMM is much more robust against the negative influence of losses, whereas the perfect lens effect is quite susceptible to losses. Finally, we have studied the effect numerically using an exact S-matrix method and realistic material parameters for a Ag/TiO₂ multilayer HMM. The numerical results show that FRET can be enhanced by two to three orders of magnitude by using a HMM instead of a thin silver film of same thickness. Since the plasmonic

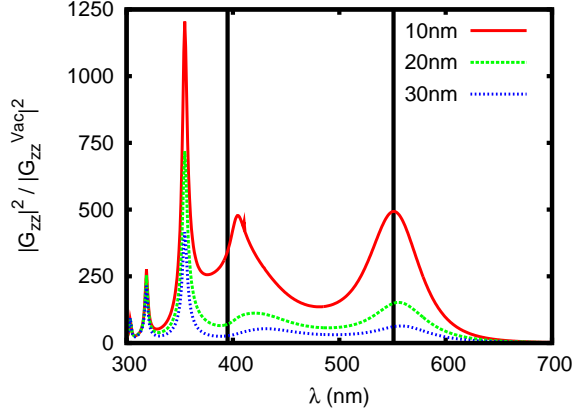
enhancement of FRET for a thin silver film has already been observed, a measurement of the enhancement due to the hyperbolic material should be feasible. Such a realization is important not only for FRET but for other areas like production of quantum entanglement [77, 78].

Acknowledgments

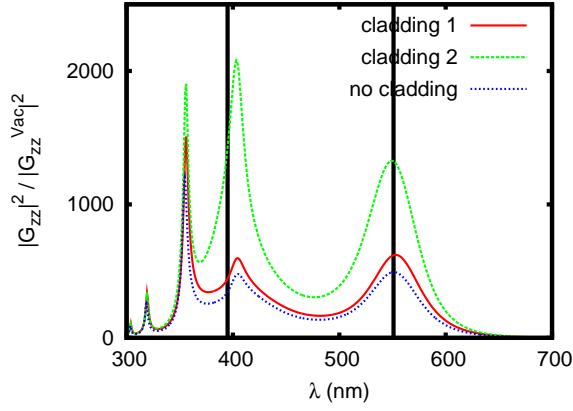
Work at CCNY was supported by the National Science Foundation (DMR-1410249).

-
- [1] P. W. Milonni, *The Quantum Vacuum*, (Academic Press, 1994).
- [2] A. I. Volokitin and B. N. J. Persson, *Rev. Mod. Phys.* **79**, 1291 (2007).
- [3] T. Förster, *Ann. Phys.* **2**, 55 (1948).
- [4] H. T. Dung, L. Knöll, and D.-G. Welsch, *Phys. Rev. A* **65**, 043813 (2002).
- [5] S.-A. Biehs and G. S. Agarwal, *J. Opt. Soc. Am. B* **30**, 700 (2013).
- [6] M. A. Nielsen and I. L. Chuang, *Quantum Computation and Quantum Information*, (Cambridge University Press, Cambridge, 2000).
- [7] I. Bouchole and K. Molmer, *Phys. Rev. A* **65**, 041803 (2002).
- [8] L. Isenhower, E. Urban, X. L. Zhang, A. T. Gill, T. Henage, T. A. Johnson, T. G. Walker, and M. Saffman, *Phys. Rev. Lett.* **104**, 010503 (2010).
- [9] G. V. Varada and G. S. Agarwal, *Phys. Rev. A* **45**, 6721 (1992).
- [10] H. R. Haakh and D. Martin-Cano, *ACS Photonics* **2**, 1686 (2015).
- [11] C. Hettich, C. Schmitt, J. Zitzmann, S. Kühn, I. Gerhardt and V. Sandoghdar, *Science* **298**, 385 (2002).
- [12] M. Saffman, T. G. Walker, T. G. and K. Molmer, *Rev. Mod. Phys.* **82**, 2313 (2010).
- [13] J. Gillet, G. S. Agarwal and T. Bastin, *Phys. Rev. A* **81**, 013837 (2010).
- [14] G. S. Agarwal and S. Dutta Gupta, arXiv:quant-ph/0011098.
- [15] R. El-Ganainy, S. John, *New J. Phys.* **15**, 083033 (2013).
- [16] P. Andrew and W. L. Barnes, *Science* **306**, 1002 (2004).
- [17] K. A. Velizhanin and T. V. Shahbazayan, *Phys. Rev. B* **86**, 245432 (2012).
- [18] G. S. Agarwal and S.-A. Biehs, *Opt. Lett.* **38**, 4421 (2013).
- [19] V. D. Karanikolas, C. A. Marocico, and A. L. Bradley, *Phys. Rev. B* **93**, 035426 (2016).
- [20] S.-A. Biehs and G. S. Agarwal, *Appl. Phys. Lett.* **103**, 243112 (2013).
- [21] A. Poudel, X. Chen, and M. A. Ratner, arXiv:1601.04338v1 (2015).
- [22] J. Li, S. K. Cushing, F. Meng, T. R. Senty, A. D. Bristow, and N. Wu, *Nat. Phot.* **9**, 601 (2015).
- [23] D. Martin-Cano, L. Martn-Moreno, F.J. Garca-Vidal, and E. Moreno, *Nano Lett.* **10**, 3129(2010).
- [24] D. Bouchet, D. Cao, R. Carminati, Y. De Wilde, and V. Krachmalnicoff, *Phys. Rev. Lett.* **116**, 037401 (2016).
- [25] C. Sönnichsen, *Plasmons in metal nanostructures*, PhD thesis (2001).
- [26] P. B. Johnson and R. W. Christy, *Phys. Rev. B* **6**, 4370 (1972).
- [27] S. Lang, H. S. Lee, A. Yu. Petrov, M. Störmer, M. Ritter, and M. Eich, *Appl. Phys. Lett.* **103**, 021905 (2013).
- [28] L. Hu and S. T. Chui, *Phys. Rev. B* **66**, 085108 (2002).
- [29] D. R. Smith and D. Schurig, *Phys. Rev. Lett.* **90**, 077405 (2003).
- [30] I. I. Smolyaninov and E. E. Narimanov, *Phys. Rev. Lett.* **105**, 067402 (2010).
- [31] Z. Jacob, I. Smolyaninov, and E. Narimanov, *Appl. Phys. Lett.* **100**, 181105 (2012).
- [32] A. N. Poddubny, P. A. Belov, and Y. S. Kivshar, *Phys. Rev. A* **84**, 023807 (2011).
- [33] A. V. Chebykin, A. A. Orlov, and P. A. Belov, *Opt. Spectr.* **109**, 938 (2010).
- [34] A. S. Potemkin, A. N. Poddubny, P. A. Belov, and Y. S. Kivshar, *Phys. Rev. A* **86**, 023848 (2012).
- [35] O. Kidwai, S. V. Zhukovsky, and J. E. Sipe, *Phys. Rev. A* **85**, 053842 (2012).
- [36] I. Iorsh, A. N. Poddubny, A. A. Orlov, P. A. Belov, and Y. S. Kivshar, *Phys. Lett. A* **376**, 185 (2012).
- [37] O. Kidwai, S. V. Zhukovsky, and J. E. Sipe, *Opt. Lett.* **36**, 2530 (2011).
- [38] A. A. Orlov, P. M. Voroshilov, P. A. Belov, and Y. S. Kivshar, *Phys. Rev. B* **84**, 045424 (2011).
- [39] J. Kim V. P. Drachev, Z. Jacob, G. V. Naik, A. Boltasseva, E. E. Narimanov, and V. M. Shalaev, *Opt. Exp.* **20**, 8100 (2012).
- [40] H. N. S. Krishnamoorthy, Z. Jacob, E. E. Narimanov, I. Kretzschmar, and V. M. Menon, *Science* **336**, 205 (2012).
- [41] T. Galfsky, H. N. S. Krishnamoorthy, W. Newman, E. E. Narimanov, Z. Jacob, and V. M. Menon, *Optica* **2**, 62 (2015).
- [42] Y. Wang, H. Sugimoto, S. Inampudi, A. Capretti, M. Fuji, and L. Dal Negro, *Appl. Phys. Lett.* **106**, 241105 (2015).
- [43] Z. Jacob, L. V. Alekseyev, E. Narimanov, *Opt. Exp.* **14**, 8247 (2006).
- [44] S. Feng and J. M. Elson, *Opt. Exp.* **14**, 216 (2006).
- [45] D. de Ceglia, M. A. Vincenti, S. Campione, F. Capolino, J. W. Haus, and M. Scalora, *Phys. Rev. B* **89**, 075123 (2014).
- [46] J. Bénédicto, E. Centeno, and A. Moreau, *Opt. Lett.* **37**, 4786 (2012).
- [47] E. Centeno and A. Moreau, *Phys. Rev. B* **92**, 045404 (2015).
- [48] D. R. Smith, P. Kolinko, and D. Schurig, *J. Opt. Soc. Am. B* **21**, 1032 (2004).
- [49] A. J. Hoffman, L. Alekseyev, S. S. Howard, K. J. Franz, D. Wasserman, V. A. Podolskiy, E. E. Narimanov, S. L. Sivco, and C. Gmachl, *Nature Mat.* **6**, 946 (2007).
- [50] C. Guclu, S. Campione, and F. Capolino, *Phys. Rev. B* **86**, 205130 (2012).
- [51] I. S. Nefedov and C. R. Simovski, *Phys. Rev. B* **84**, 195459 (2011).
- [52] S.-A. Biehs, M. Tschikin, P. Ben-Abdallah, *Phys. Rev. Lett.* **109**, 104301 (2012).
- [53] Y. Guo, C. L. Cortes, S. Molesky, and Z. Jacob, *Appl. Phys. Lett.* **101**, 131106 (2012).

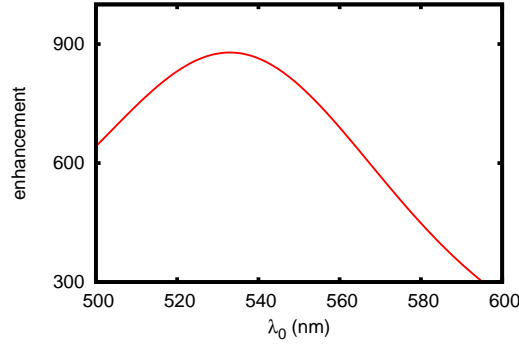
- [54] S.-A. Biehs, M. Tschikin, R. Messina, and P. Ben-Abdallah, *Appl. Phys. Lett.* **102** 131106 (2013).
- [55] J. Shi, B. Liu, P. Li, L. Y. Ng, and S. Shen, *Nano Letters* **15**, 1217 (2015).
- [56] S.-A. Biehs, S. Lang, A. Yu. Petrov, M. Eich, and P. Ben-Abdallah, *Phys. Rev. Lett.* **115**, 174301 (2015).
- [57] C. L. Cortes and Z. Jacob, *Frontiers in Optics 2013/Laser Science XXIX* (2013).
- [58] W. Newman, C. Cortes, D. Purschke, A. Afshar, Z. Chen, G. De los Reyes, F. Hegmann, K. Cadien, R. Fedosejevs, and Z. Jacob, *CLEO 2015* (2015).
- [59] D. W. Thompson, M. J. DeVries, T. E. Tiwald, and J. A. Woollam, *Thin Solid Films* **313-314**, 341 (1998).
- [60] J. D. Caldwell, A. Kretinin, Y. Chen, V. Giannini, M. M. Fogler, Y. Francescato, C. T. Ellis, J. G. Tischler, C. R. Woods, A. J. Giles, M. Hong, K. Watanabe, T. Taniguchi, S. A. Maier, K. S. Novoselov, arXiv:1404.0494.
- [61] M. Esslinger, R. Vogelgesang, N. Talebi, W. Khunsin, P. Gehring, S. de Zuani, B. Gompf, and K. Kern, *ACS Photonics*, **1**, 1285(2014).
- [62] E. E. Narimanov and A. V. Kildishev, *Nature Photonics* **9**. 214 (2015).
- [63] K. Korzeb, M. Gajc, and D. A. Pawlak, *Opt. Expr.* **23**, 25406 (2015).
- [64] R. Fleury and A. Alú, *Phys. Rev. B* **87**, 201101(R) (2013).
- [65] M. Silveirinha and N. Engheta, *Phys. Rev. Lett.* **97**, 157403 (2006).
- [66] B. Edwards, A. Alú, M. E. Young, M. Silveirinha, and N. Engheta, *Phys. Rev. Lett.* **100**, 033903 (2008).
- [67] J. B. Pendry, *Phys. Rev. Lett.* **85**, 3966 (2000).
- [68] J. I. Gersten and A. Nitzan, *Chem. Phys. Lett.* **104**, 31 (1984).
- [69] M. L. Viger, D. Brouard, and D. Boudreau, *J. Phys. Chem. C* **115**, 2974 (2011).
- [70] X. Zhang, C. A. Marocico, M. Lunz, V. A. Gerard, Y. K. Gunko, V. Lesnyak, N. Gaponik, A. S. Susha, A. L. Rogach, and A. L. Bradley, *ACS Nano* **8**, 1273 (2014).
- [71] P. Yeh, *Optical Waves in Layered Media*, (John Wiley & Sons, New Jersey, 2005).
- [72] P. A. Belov, C. R. Simovski, and P. Ikonen, *Phys. Rev. B* **71**, 193105 (2005).
- [73] P. A. Belov and Y. Hao, *Phys. Rev. B* **73**, 113110 (2006).
- [74] M. Tschikin, S.-A. Biehs, R. Messina, P. Ben-Abdallah, *J. Opt.* **15**, 105101 (2013).
- [75] M. Auslender and S. Have, *Opt. Lett.* **21**, 1765 (1996).
- [76] J. R. Devore, *J. Opt. Soc. Am.* **41**, 416 (1951).
- [77] See Sec. 15.3 of G. S. Agarwal, *Quantum Optics*, (Cambridge University Press, Cambridge, 2012).
- [78] S.-A. Biehs and G. S. Agarwal, preprint.
- [79] For the numeric integration we use a cutoff at $\kappa = 300/(z - z')$ which is much larger than the intrinsic cutoff of the integrand at $\kappa \approx 1/(z - z' - d)$.



(a) $z' = -10$ nm, -20 nm, -30 nm and $z - d = 10$ nm, 20 nm, 30 nm



(b) Influence of a cladding



(c) Influence of the line shapes of the acceptor and donor on the enhancement factor

Figure 9: Plot of F_z for a Ag/TiO₂ multilayer structure with $N = 24$ for different donor-acceptor positions in (a). In (b) we show for $z' = -10$ nm the influence of a silica cladding of 10nm thickness which is deposited on the metal layer on the side of the donor. The donor lies on top of the cladding and the acceptor is set at position $z - d = 10$ nm (cladding 1) and $z - d = 0$ nm (cladding 2). Note that the TiO₂ layer functions as a cladding on the acceptor side of the hyperbolic structure so that by setting $z - d = 0$ nm the acceptor just lies on top of this 'cladding'. In (c) we have plotted the enhancement factor defined in Eq. (29) as a function of the maximum emission wavelength λ_0 of the donor while the acceptor wavelength is $\bar{\lambda} = \lambda_0 + 30$ nm for the configuration 'cladding 2' in (b).

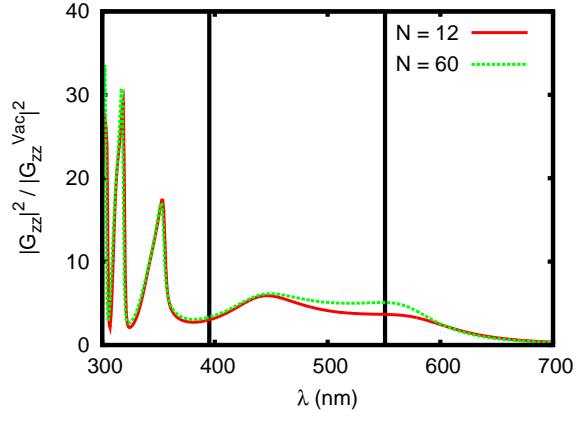
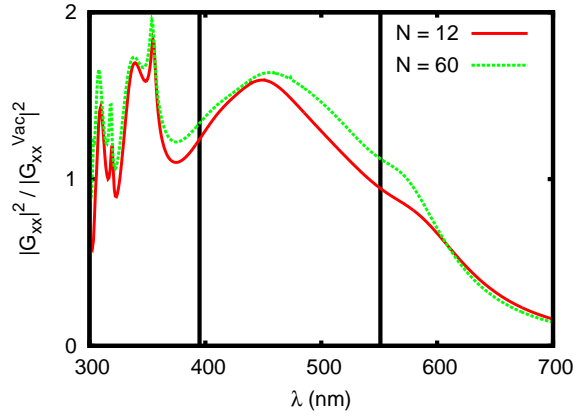
(a) Ag/TiO₂, F_z (b) Ag/TiO₂, F_x

Figure 10: Same as in Fig. 8 but with $z' = -100$ nm and $z = d + 100$ nm for $N = 12, 60$. The EMT result is not shown because it practically coincides with the result for $N = 60$.